Journal of Geophysical Research: Atmospheres

RESEARCH ARTICLE
10.1029/2018JD028272

Retrieval of Atmospheric Profiles in the New York State Mesonet Using One-Dimensional Variational Algorithm

Jun Yang[1,2] **and Qilong Min**[2]

[1]Chinese Academy of Meteorological Sciences, State Key Laboratory of Severe Weather, Beijing, China, [2]State University of New York, Atmospheric Sciences Research Center, Albany, NY, USA

Key Points:
- A one-dimensional variational algorithm was developed to retrieve temperature and water vapor density profiles under clear-sky conditions
- The results of the proposed algorithm outperform the neural net retrievals and the Rapid Refresh reanalysis
- The temperature profiles are improved mainly in the low atmosphere, while the humidity profiles are improved at almost all levels

Correspondence to:
Q. Min,
qmin@albany.edu

Citation:
Yang, J., & Min, Q. (2018). Retrieval of atmospheric profiles in the New York State Mesonet using one-dimensional variational algorithm. *Journal of Geophysical Research: Atmospheres*, *123*, 7563–7575. https://doi.org/10.1029/2018JD028272

Received 3 JAN 2018
Accepted 30 MAY 2018
Accepted article online 7 JUN 2018
Published online 26 JUL 2018

Abstract A one-dimensional variational (1DVAR) algorithm was developed, which combines measurements taken by the ground-based microwave radiometer profiler (MWRP) with the Rapid Refresh (RAP) model to retrieve a more accurate temperature and humidity profiles under clear sky. The passive and active microwave-vector radiative transfer model was used to simulate brightness temperatures and calculate weighting functions for 22 channels of the MWRP. As MWRP measurements are mainly weighted in the lower atmosphere, a measurement adjustment is performed to reduce the contribution from above 10 km. The results of the 1DVAR algorithm have been compared with the MWRP built-in neural network (NN) retrievals and radiosonde observations, which show that the 1DVAR method outperforms the NN retrieval both in temperature and water vapor. Our statistical study further shows that the water vapor profiles from RAP are biased higher than the radiosonde observations, while the 1DVAR-retrieved humidity values show significant improvements throughout the entire 10-km range. The improvements in temperature profiles occur mainly within the lowest 4-km atmosphere, while upper level retrievals are mostly influenced by initial values. This is consistent with the characteristics of the Jacobian matrix and the background error covariance matrix. The outcomes of 44 clear-sky cases show that the maximum mean retrieval error of the 1DVAR algorithm is less than 0.2 K for temperature below 4 km and less than 0.15 g/m^3 in water vapor density. These results are shown to be significantly better than the NN retrieval (3.0 K and 1.25 g/m^3) and also superior to the RAP reanalysis (0.3 K and 0.5 g/m^3).

1. Introduction

High-quality measurements of upper atmospheric conditions such as temperature, humidity, and pressure are crucial for accurate weather forecasting. Therefore, it is necessary to develop numerical weather prediction models capable of producing high-resolution upper atmospheric profiles. Radiosonde observations (RAOBs) take direct measurements of temperature, moisture, and pressure with a high degree of accuracy up to an altitude of roughly 30 km. However, RAOB measurements are only taken twice daily at selected locations (New York State [NYS] has three sites totaling in only six sounding profiles per day). In order to improve the temporal and spatial resolutions of sounding data, various approaches based on passive infrared or microwave spectral radiation measurements and active lidar measurements have been proposed and implemented. Such systems are cost-effective and able to rapidly retrieve atmospheric profiles throughout a given 24-hr period (Blumstein et al., 2004; Boukabara et al., 2011; Jang et al., 2017; Sanò et al., 2015).

The microwave radiometer (MWR), which operates in the range of 20–60 GHz, possesses the potential to provide continuous retrievals of temperature and water vapor profiles with a relatively high temporal resolution. The statistical inversion methods, such as regression (Westwater, 1993), Bayesian maximum probability (Keihm & Marsh, 1996), and neural network (NN, Cadeddu et al., 2009), had been applied in the past to derive such profiles. These methods combined the measurements of MWR with radiosonde climatology near the observation site or with various model outputs. Solheim et al. (1998) compared the advantages and disadvantages of these statistical inversion methods in detail. Overall, these methods have great limitations on solving nonlinear problems and their successful operation relies on a large number of training samples.

The one-dimensional variational (1DVAR) approach is a physical inversion method which utilizes a precise forward radiative transfer model and iterations to search for an optimal solution while simultaneously minimizing the cost function. Several studies have shown that this method achieves better inversion accuracy than

traditional statistical methods (Cimini et al., 2010; Duncan & Kummerow, 2016; Hewison, 2007). The accuracy of the first guess is an important factor affecting retrievals of the 1DVAR method. Most studies adopted the results of numerical forecast model outputs as the initial values of the 1DVAR algorithm. The European Centre for Medium-scale Weather Forecast and the National Center for Environmental Prediction's (NCEP) global forecasts are two of the most commonly used a priori information. Both satellite-based and ground-based MWRs can be applied to retrieve atmospheric profiles using the 1DVAR method by combining the results of numerical forecasting models. Liu and Weng (2005) used the 1DVAR algorithm to derive the atmospheric vertical profiles of temperature, humidity, and liquid water from instrument measurements of the advanced microwave sounding units. Hewison (2007) introduced the 1DVAR retrieval of temperature, water vapor, and cloud profiles from a 12-channel ground-based MWR. In the above methods, the a priori information adopted by the researchers is mostly 6 or 12-hr numerical forecast model outputs; such methods provide limited forecast accuracy (Benjamin et al., 2016). To improve retrieval results, Cimini et al. (2011) adopted the U.S. National Oceanic and Atmospheric Administration Local Analysis and Prediction System's hourly analysis as the background information in their 1DVAR retrieval for the 2010 Winter Olympics. Martinet et al. (2017) introduced temperature profile retrievals in an Alpine valley by merging brightness temperature measurements from the ground-based MWR with 1-hr forecasts from the convective scale model. Recently, NCEP has developed a new operational hourly updated numerical weather prediction system, the Rapid Refresh (RAP), covering all of North America (Benjamin et al., 2016) which allows for more accurate a priori information on the current atmospheric state.

The State University of New York, University at Albany, in partnership with the Federal Emergency Management Agency, the NYS Division of Homeland Security and Emergency Services, and the National Weather Service, has developed an advanced statewide Mesonet equipped with sophisticated instrumentation to detect high-impact weather phenomena. The NYS Mesonet consists of a 126-station network across the state, with an average spacing of about 25 km. Each Mesonet site provides a "standard" suite of measurements including surface temperature, relative humidity, wind speed and direction, precipitation, solar radiation, atmospheric pressure, and soil moisture and temperature at three depths. Of the 126 sites, 17 sites are "enhanced" or outfitted with additional, specialized instrumentation including an environmental sky imager-radiometer (eSIR) that measures accurate spectral solar radiation distribution, cloud cover distribution and motion, a Doppler lidar measuring 3-D winds in the vertical up to 1–2 km aboveground level, and a MWR profiler (MWRP) providing vertical profiles of temperature and moisture up to 10 km aboveground level. The retrieval results of MWRP are based on its built-in NN model, which can only provide limited retrieval accuracy. Improving the NN configuration (Blackwell, 2005) is a feasible option to enhance the instrument's inversion ability. However, the NN algorithm has its limitations, including ambiguous physical meanings and the need for large amounts of historical sounding data to train network parameters. To utilize MWRP measurements for vertical profiles of temperature and moisture, a new 1DVAR method has been developed which combines observations from the ground-based MWRP with the forecasted profiles (reanalysis) of the RAP. The ground-based MWRP and the RAP data are introduced in section 2. Section 3 presents the basic concept of the 1DVAR retrieval method. Section 4 describes the results of the 1DVAR retrieval algorithm developed for the NYS Mesonet in detail. The conclusions and suggestions for future research are discussed in section 5.

2. Instrument and Data

Microwave radiometer profilers used in the NYS Mesonet observe absolute microwave radiances (or brightness temperatures) at 22 frequencies. Channels 1–8 are in the range of 22–30 GHz, and the remaining 14 channels fall within the 51–60 GHz range. The center frequencies of the first eight channels are 22.234, 22.500, 23.034, 23.834, 25.000, 26.234, 28.000, and 30.000 GHz, most of which are sensitive to atmospheric water vapor and are used to derive the humidity profile. The remaining 14 channels are located within oxygen absorption bands and their center frequencies are 51.248, 51.760, 52.280, 52.804, 53.336, 53.848, 54.400, 54.940, 55.500, 56.020, 56.660, 57.288, 57.964, and 58.800 GHz. An MWRP has been installed on the roof of the Atmospheric Sciences Research Center (ASRC; 42.6921°N, 73.8326°W, 95 m above the sea level) since the end of 2016. The MWRP can measure the brightness temperatures at any zenith angle every few minutes. During the MWRP observations, operational radiosonde balloons were launched routinely at UTC 00:00 and 12:00 from the ASRC site. Equipped about 10 m away from the MWRP is an eSIR developed by scientists at

University at Albany to obtain real-time images of the sky and spectral solar radiation which can be used to determine current sky condition by automatic cloud detection algorithms (Yang et al., 2016, 2017).

The atmospheric state vectors retrieved in this study are profiles of water vapor density (g/m^3) and temperature under clear-sky conditions. We divide the atmosphere (at 0–10 km height range) into 40 layers, each with a depth of 250 m. After proper calibration, the MWRP equipment located on the roof of the ASRC has provided stable atmospheric radiation data at 22 microwave channels since April 2017. Its radiation output in the zenith direction are used as our measurements. The initial atmospheric state vectors extracted from the NCEP developed RAP are a continental-scale operational, hourly renewed analysis/modeling system. The RAP assimilates multiple data sources such as surface observation, radar data, satellite data, balloon data, and aircraft weather data to generate hourly forecasts of up to 18 hr in advance. The horizontal resolution of each grid point is 13 km, and its vertical direction is divided into 50 layers extending from the surface to a height of 10 hPa. Profile data can be extracted from the RAP using a bilinear interpolation algorithm by inputting the latitude and longitude of the ASRC site. The extracted profile includes air pressure, temperature, and specific humidity (kg/kg) at 50 different hybrid layers. To get the RAP parameters on the same 40 layers as the inversion, we use atmospheric pressure matching to calculate the position of 40 pressure layers in RAP, and then the linear interpolation algorithm is adopted to get the temperature and specific humidity of each layer. By converting specific humidity to water vapor density, we can derive water vapor initial values at each of the 40 layers. The clear-sky samples are determined by combining the eSIR measured sky images with sounding observations. A total of 44 clear-sky cases between April and June 2017 are used to evaluate the inversion accuracy of the 1DVAR algorithm in this study.

3. 1DVAR Retrieval Algorithm

The 1DVAR retrieval method consists of two key components: One is the accurate forward radiative transfer model to simulate radiation brightness temperatures and calculate weighting functions (or Jacobian matrix); the other is a method to minimize a cost function, which represents the total errors of the observation field and background information.

The forward model adopted in this study is the passive and active microwave-vector radiative transfer (PAM-VRT) model (Yang & Min, 2015), which is composed of five components: gas absorption, hydrometeor particle properties, surface emissivity, microwave vector radiative transfer of successive order of scattering, and passive and active microwave sensor simulators. The gaseous absorption module in the PAM-VRT can simulate optical depth and brightness temperature for any frequency within the microwave range by adopting either a line-by-line physical model or several fast models such as Liebe's atmospheric millimeter wave propagation models (Abbreviated as Liebe89 and Liebe93, respectively; Liebe, 1989; Liebe et al., 1993) and Rosenkranz's updated models (abbreviated as Rosen98 and Rosen02; Rosenkranz, 1998).

To evaluate the gas absorption models, we simulated brightness temperatures of the MWRP 22 channels within the lowest 30-km atmosphere for all 44 clear-sky cases. Based on MWRP specifications, the accuracy of brightness temperature for each channel should be within 0.3 K after an exceptionally accurate calibration (Liljegren, 2000). However, as shown in the left panel of Figure 1, the average biases of the observations minus the simulations range from 2.0 to 3.0 K for all five gas absorption models, especially in the water vapor bands and low frequencies of the oxygen bands. It is clear that the differences between gas absorption models are less than 1 K. Hence, the main reason for these biases may be due to the uncertainty of the instrument calibration or some other errors (Cimini et al., 2011). We also calculated the average deviations of the five gas absorption models in all channels. The results show that the Liebe89 model possesses a relatively superior simulation capability; similar conclusions can be found at Rosenkranz (1998) and Lin et al. (2001). The mean deviation between the simulation values of Liebe89 and the MWRP measurements is only −0.0911 K, although the maximum bias of a certain channel still reaches ±2 K. Therefore, we chose Liebe89 as the forward gas absorption model in the 1DVAR retrieval algorithm. Using this model, we simulated atmospheric radiations within the lowest 30 and 10 km, respectively. The radiation differences between 30 and 10-km atmospheres for each channel are shown as the red line in the right panel of Figure 1, which indicates that the differences are between 0.4 and 0.6 K in the water vapor bands, between 0.1 and 7.5 K in the first nine oxygen bands (low frequencies), and very close to zero in the remaining five oxygen channels. The difference between simulated radiations within the lowest 10 km and observations is represented with the black line in

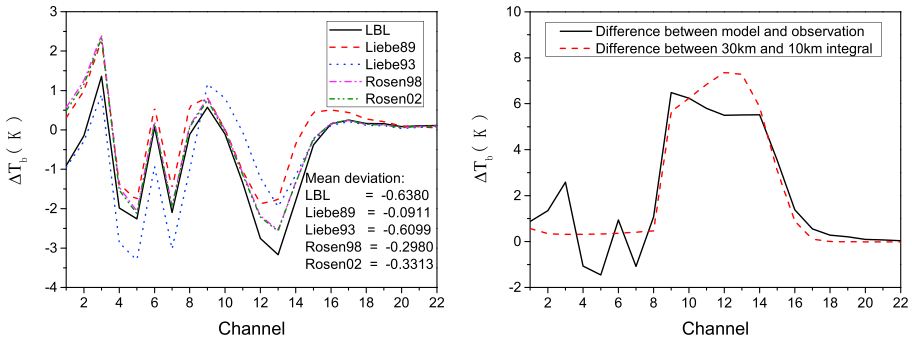

Figure 1. The biases between models and observations. (left) Average biases of the observations minus the simulations in each channel using five different gas absorption models. (right) Bias between observations and Liebe89 model which only adopts the lowest 10-km atmosphere.

the right panel of Figure 1. The new (background removed) observations represent the radiations below 10 km and can be obtained by subtracting the integrated difference from the original observations. Next, the new observations will serve as our observation field while considering only the radiations below 10 km in the forward simulation.

The weighting function, which represents the sensitivity of a component at different heights for each wavelength (Araki et al., 2015), can be computed in the PAM-VRT model for temperature sensitive channels and water vapor absorption bands, respectively. By setting a slight change in the temperature (ΔT) of each layer, the perturbation variance of brightness temperature (ΔF) can be simulated using the PAM-VRT model. The ratio, $\Delta F/\Delta T$, is called the Jacobian matrix of the temperature profile. The same method can be applied to calculate the Jacobian matrix of the water vapor density profile. The difference is that we compute the change of the water vapor density in natural logarithm form ($\Delta \ln \rho_v$; Cimini et al., 2011). Figure 2 shows the Jacobian matrices for the water vapor and temperature channels, respectively. In calculating the Jacobian matrices, the increment of each layer is the initial value multiplied by 1% for temperature and 0.01 in $\ln\rho_v$.

The background error covariance matrices B can be estimated using the RAP reanalysis data which represents the error between the background state vector and the average atmospheric state. Based on the RAP reanalysis data of 44 clear-sky cases, a 44-by-40 background matrix can be constructed, and the covariance of the matrix is the estimated background error covariance matrix B with a size of 40-by-40. Figure 3 shows the background error covariance matrices for all 44 cases. The temperature error covariance matrix has a large error at lower levels, especially below 4 km, while the maximum error appears at midlevels in the water vapor error covariance matrix. This is mainly a result of the logarithmic processing of water vapor which will serve to increase high-level error while reducing low-level error.

Based on the atmospheric profile of the background or a priori information, the simulated downward radiations or brightness temperatures can be obtained using the forward Liebe89 model for the specified frequencies. Combined with measurements of brightness temperature from a ground-based MWRP, the 1DVAR retrieval method can return the most likely atmospheric state. Assuming that both errors in observation and background have a typical Gaussian distribution (Desportes et al., 2010; Liu & Weng, 2005), the optimal estimation of the atmospheric profile is equivalent to solving the minimum value of the cost function, $J(X)$, which can be written as

$$J(X) = \frac{1}{2}(X - X_0)^T B^{-1}(X - X_0) + \frac{1}{2}(Y - Y(X))^T R^{-1}(Y - Y(X)) \quad (1)$$

Here B is the error covariance matrix of the background or a priori profile X_0 and R represents the total errors associated with sensor noise as well as in the covariance matrix of the forward model. Y denotes the observed brightness temperatures, and $Y(X)$ is the simulated brightness temperatures for the specified frequencies of the state profile, X. Superscripts -1 and T represent inverse and transpose, respectively.

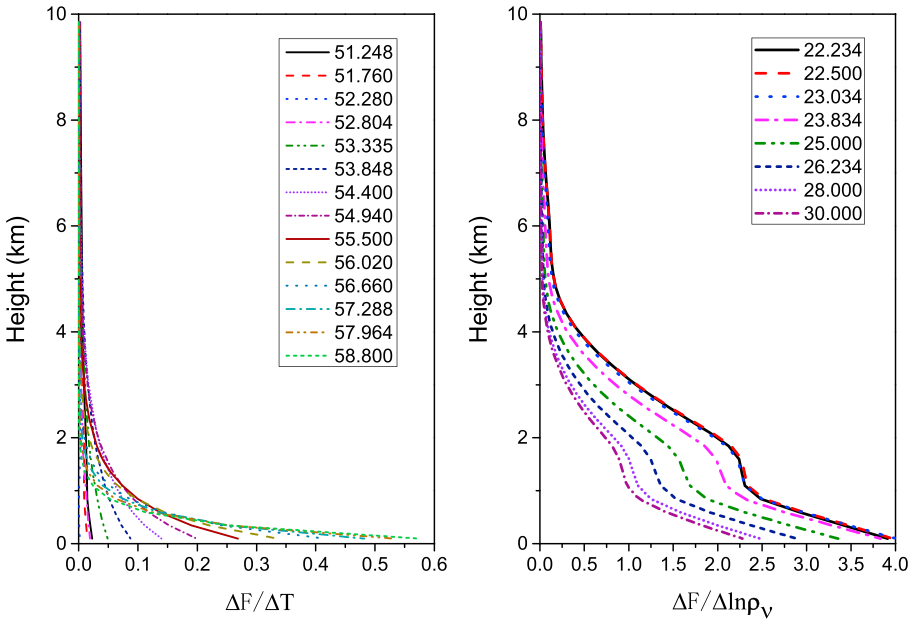

Figure 2. Jacobian matrices for the Rapid Refresh state profiles at UTC 12:00, 1 June 2017. (left) Fourteen temperature channels and (right) 8 water vapor channels.

There are two different variational iterations which solve the minimization of $J(X)$ (Rodgers, 1976),

$$X_{n+1} = X_0 + BK_n^T\left(K_nBK_n^T + \mathrm{R}\right)^{-1}[(Y - Y(X_n)) + K_n(X_n - X_0)] \tag{2}$$

$$X_{n+1} = X_0 + \left(B^{-1} + K_n^TR^{-1}K_n\right)^{-1}K_n^TR^{-1}[(Y - Y(X_n)) + K_n(X_n - X_0)] \tag{3}$$

where X_n represents the nth estimate of the atmospheric state; K is the Jacobian matrix, which is the derivative of the observation vector Y with respect to the state vector X.

When the number of profile elements is larger than that of observation channels (that is to say, the R matrix is smaller than the B matrix), equation (2) should be used (Liu & Weng, 2005). Contrarily, if there are more measurements than the unknown profile elements, equation (3) should be considered for atmospheric profile retrieval. Equation (3) can be solved using the Levenberg-Marquardt formula with fast convergence (Culverwell et al., 2015; Rodgers, 2000). However, both 14 channels for retrieving temperature profile and 8 channels for inversion of water vapor profile are much smaller than the number of the atmospheric profile layers, so the iteration equation (2) is used to solve the minimization of $J(X)$ in this study. The

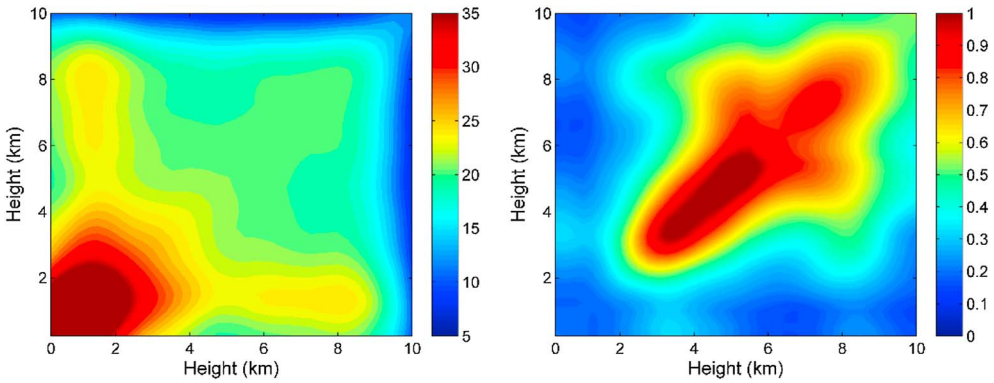

Figure 3. Estimated background error covariance matrices for all 44 cases. (left) Temperature error covariance and (right) water vapor error covariance.

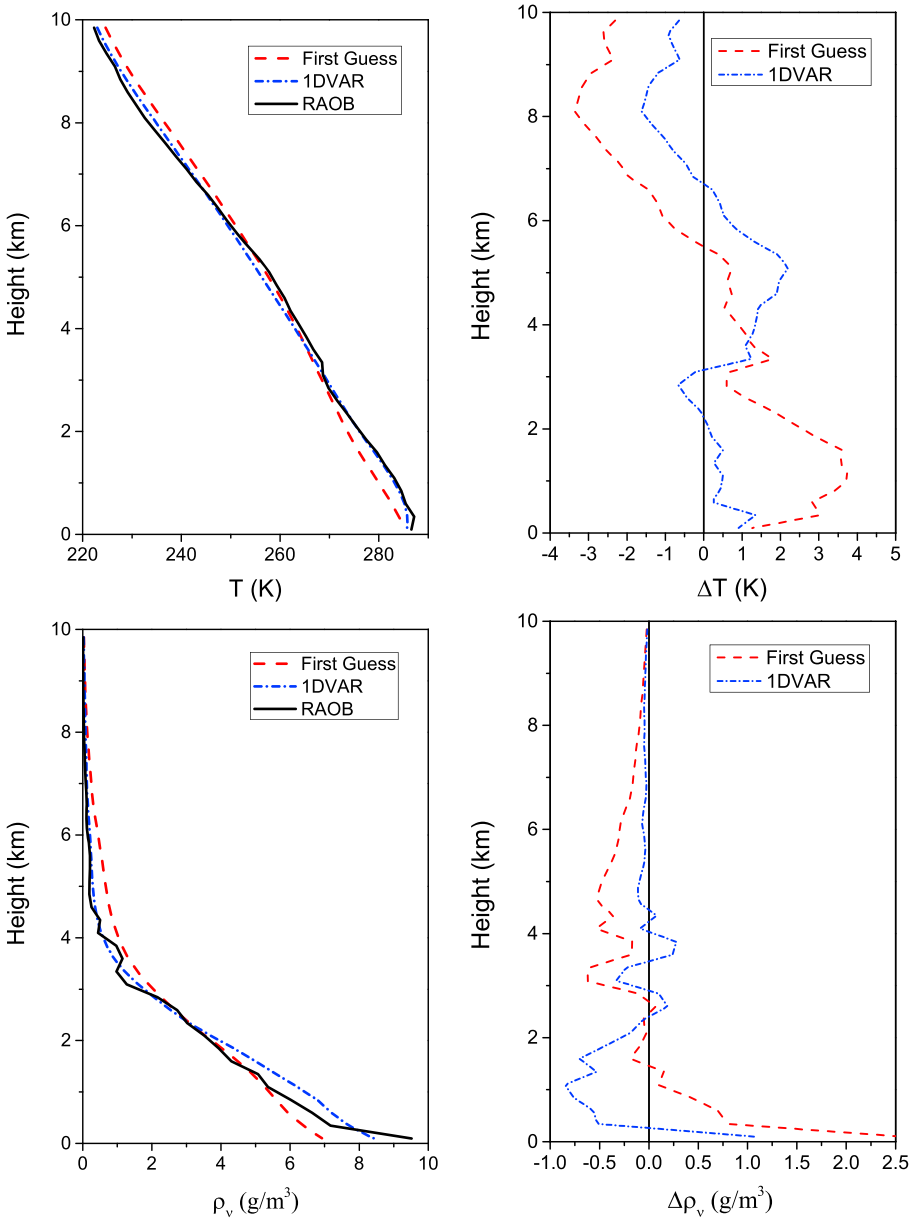

Figure 4. The inversion test with the average atmospheric state as the first guess for the case of UTC 12:00, 1 June 2017. (top row) Temperature retrieval and its inversion error and (bottom row) inversion of water vapor density and its retrieval error.

convergence iteration terminates when the change of cost function is very small or when it reaches the maximum iteration setting.

To evaluate and validate the 1DVAR algorithm, we performed an inversion test for the case at UTC 12:00, 1 June 2017. In this test, the average atmospheric state of the 44 cases was used as the initial value (or first guess) of the 1DVAR algorithm. Although there is a large deviation between the first guess and the true values (RAOBs) for both temperature and water vapor profiles, the inversion results of the 1DVAR algorithm are satisfactory (see Figure 4). In particular, the temperature profile of the inversion has a good agreement with the RAOB in lower layers, and the retrieval water vapor profile has been greatly improved both in the lower and upper layers. The results of the inversion are in agreement with the characteristics of the weighting functions and the estimated background error covariance matrices. For the Jacobian matrix of the oxygen channels, their weights reach peak values near the surface and then decrease rapidly within a few

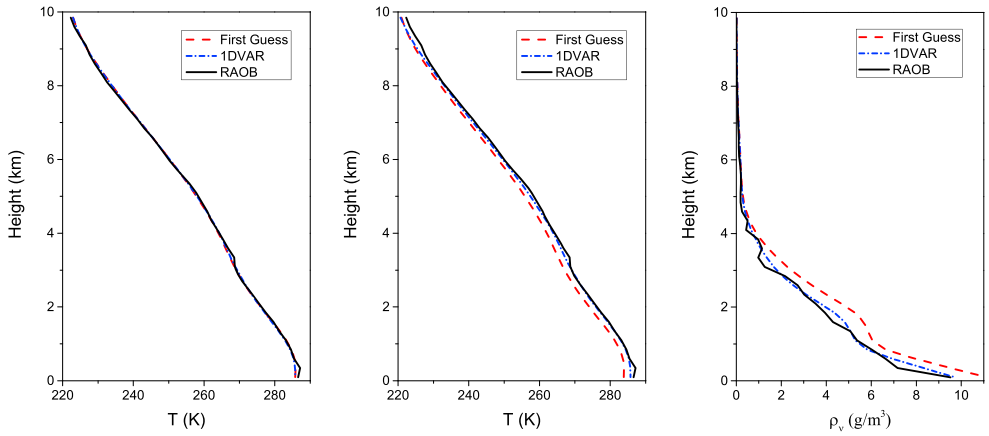

Figure 5. The inversion results with the Rapid Refresh (RAP) reanalysis as the first guess for the case of UTC 12:00, 1 June 2017. (left) Temperature retrieval, (middle) temperature retrieval but with initial values randomly 1–2 K smaller than the RAP reanalysis, and (right) inversion of water vapor density.

kilometers. In the background error covariance matrix of the temperature profiles, the low-level error is also significantly larger than the upper level. Unlike that of the temperature profile, the Jacobian matrix of the humidity profile has a certain sensitivity to changes in humidity at different heights. The inversion results are optimized for the initial humidity profile in most of the altitude levels.

4. Results

Based on the information of the observation field, the above inversion test shows that our 1DVAR algorithm is feasible and that the retrieval algorithm continuously adjusts the initial field. In practice, we will use the corresponding RAP reanalysis/forecast data as the initial field. Figure 5 shows the inversion results with the RAP reanalysis as the first guess for the same case as shown in Figure 4. As the first guess from RAP reanalysis is very close to the profile of the RAOB, it is difficult to determine whether the high inversion accuracy is caused by the good initial value or by the accurate 1DVAR algorithm. To better illustrate the effectiveness of the 1DVAR algorithm, we randomly subtract 1–2 K from the original RAP temperature profile and use it as the initial value to retrieve temperature. The inversion result shows that the temperature profile at the lower level still yields a good inversion accuracy, indicating that the retrieval is insensitive to the initial guess where information of MWRP measurements prevails. Unlike the temperature profile, there is a relatively large deviation between the water vapor profiles of the RAP reanalysis and the RAOB, especially within lower levels. For the inversion of water vapor density, the 1DVAR algorithm converges to a solution close to the RAOB profile (see right panel of Figure 5).

For all following discussion on 1DVAR temperature profile inversion, we used two different initial values to evaluate the performance of the proposed algorithm. The first one used the original RAP reanalysis as the first guess, and its retrieval result is expressed as 1DVAR 1. The second initial value has a greater deviation from the RAOB profile than that of the first, which is equal to the RAP temperature profile minus 1–2 K, randomly, at each height level. This retrieval result is represented as 1DVAR 2. Furthermore, we also included the vendor's statistical retrievals of NN for comparison. The initial temperature profile is very close to the true profile when RAP reanalysis is adopted as the initial guess. The inversion can be considered as a relative linear adjustment with almost all cases converging after 1 to 2 iterations. For water vapor inversion, the linearity between the initial value and the true value is relatively poor. Most of the cases need 4 to 5 iterations to converge.

From the temperature inversion results of several cases (see top row of Figure 6), the NN retrievals have a large deviation from the RAOBs, which are significantly lower than the true values at almost all height levels. Both the 1DVAR 1 and 1DVAR 2 inversions obtained a high level of inversion precision within low levels. Meanwhile, as a result of more accurate initial values, the 1DVAR 1 retrieval obtained a higher degree of accuracy within the upper levels than that of the 1DVAR 2. Similar to the temperature inversion, the NN retrievals for water vapor density also have a large deviation from the RAOBs. The difference is that at lower levels the

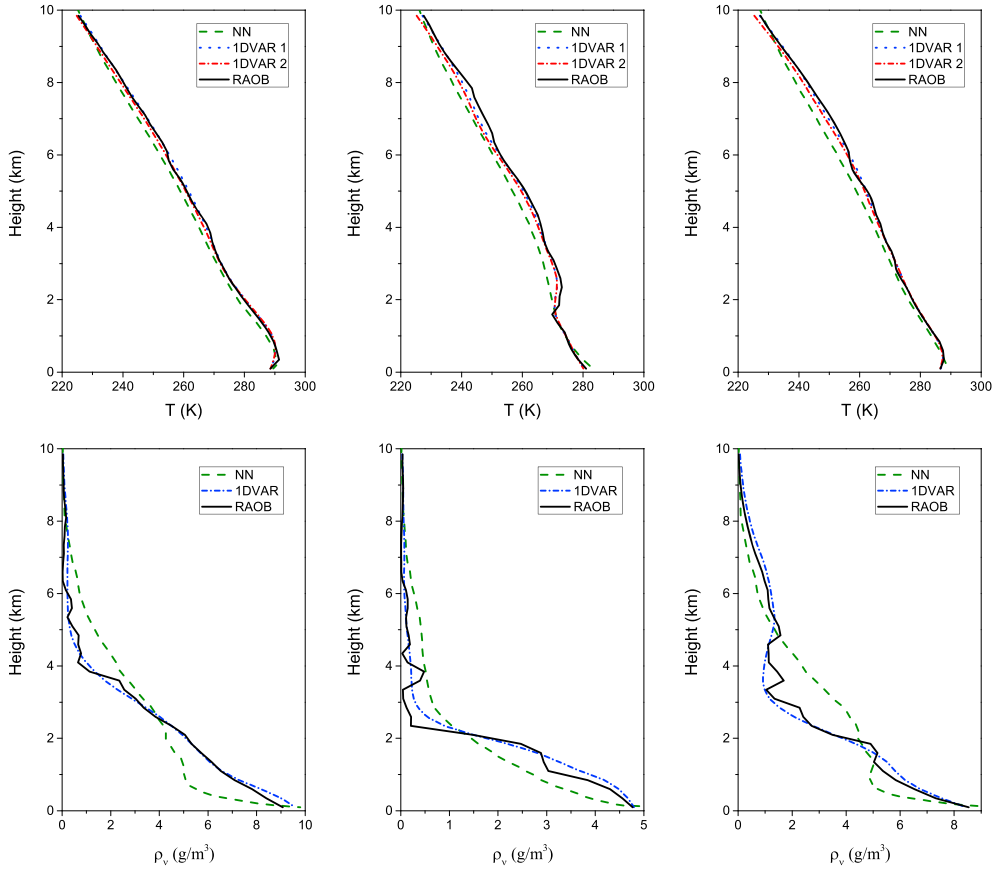

Figure 6. Comparison of neural network and one-dimensional variational retrievals with respect to radiosonde observations for several cases. (top row) Temperature inversion and (bottom row) inversion of the water vapor density. (left column) Case of UTC 12:00, 16 April 2017; (middle column) case of UTC 12:00, 11 May 2017; and (right column) case of UTC 12:00, 24 May 2017.

results of the NN algorithm are significantly smaller than those of the RAOB, while at upper levels the results are greater than the RAOB. In contrast, the retrievals of the 1DVAR, which fully merged the accuracy of the initial values with observations of MWRP, achieved better performance throughout the entirety of the vertical height. It should be noted that the 1DVAR algorithm still missed some details such as the dramatic

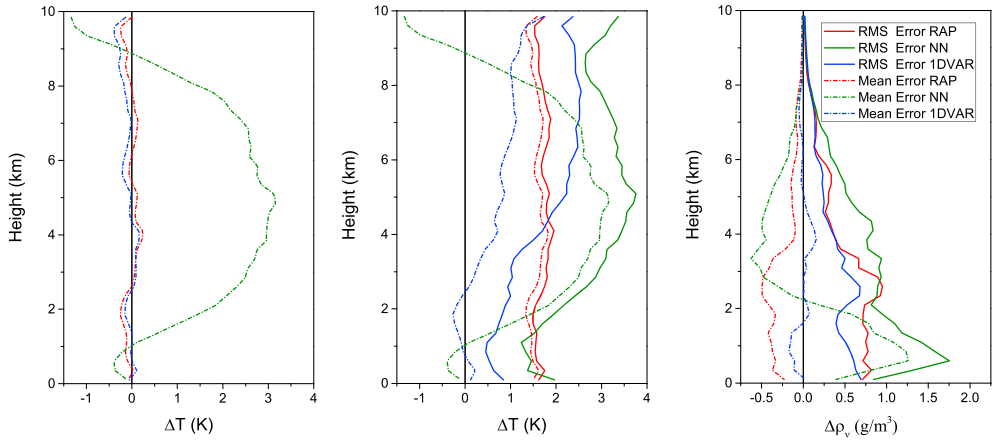

Figure 7. The statistical errors of the inversion results for all 44 cases. (left) Mean errors of temperature, (middle) mean and rms errors of temperature, and (right) mean and rms errors of water vapor density.

Table 1
The Errors of Precipitable Water Vapor Between Three Methods and Radiosonde Observations for 44 Cases (mm)

	Maximum error	Minimum error	Mean error	rms error
Rapid Refresh	9.73	−1.54	1.92	2.69
Neural network	13.80	−3.09	−0.03	2.39
One-dimensional variational	1.07	−0.69	0.09	0.45

changes in humidity (see bottom row of Figure 6). This may be due to the fact that the smooth weighting function has a very limited inversion ability to resolve those turning points.

The statistical errors of the inversion results for 44 cases are summarized in Figure 7. The maximum deviation between the original RAP temperature profile and RAOB is about 0.3 K. The 1DVAR algorithm achieves a better temperature inversion accuracy below 4 km with a maximum mean error of less than 0.2 K. The temperature inversion results of the NN have a greater deviation throughout nearly the entire vertical height with a maximum error greater than 3 K. The middle panel of Figure 7 shows the mean and root mean square (rms) errors for the RAP, NN, and 1DVAR, in which the temperature profiles of RAP, adopted as the initial value in the 1DVAR algorithm, are reduced 1–2 K randomly at each layer for all cases. Although the mean error of the initial value, in terms of the temperature inversion, is between 1 and 2 K, the mean error of the 1DVAR inversion is less than 1 K at most levels. The rms error of the 1DVAR temperature profile has also been greatly improved, especially below 4 km, which is consistent with the characteristics of the temperature profile's weight functions and background error covariance. The statistical errors for water vapor density are shown in the right panel of Figure 7. Similar to the temperature profile retrievals, the NN retrieval has the greatest error both for mean and rms. The mean error of the NN indicates that the result of its inversion is lower than the RAOB below 2 km and higher than the RAOB above that level. The maximum deviation of the NN occurs at about a height of 1 km with a maximum mean error of 1.25 g/m^3 and a maximum rms error of 1.75 g/m^3. The inversion errors of the 1DVAR algorithm are significantly improved compared with the RAP profile at almost all height levels. The maximum mean error and rms error are 0.15 and 0.7 g/m^3, respectively.

To better evaluate the accuracy of the water vapor inversion, we integrated the water vapor density in the range of 0–10 km and converted it to precipitable water vapor (PWV) for 44 cases based on the RAP, NN, 1DVAR, and RAOB, respectively. Taking the PWV of RAOB as the standard value, the differences between the three methods (RAP, NN, and 1DVAR) and RAOB were calculated. Their statistical results are given in Table 1, which shows that the MWRP built-in NN algorithm has the smallest average error with RAOB. Several studies (Cadeddu et al., 2009; Mattioli et al., 2008) had also shown that the MWRP has a good inversion capability for PWV. The mean error of the 1DVAR method is also small, and its rms error is still very small. The RAP has both the biggest mean error and rms error among three methods, which indicates that the RAP overestimates the PWV.

To further evaluate the 1DVAR algorithm, we performed a continuous inversion with a time resolution of 20 min using the MWRP observations on 22 June 2017. The total sky images per hour from UTC 9:00 to

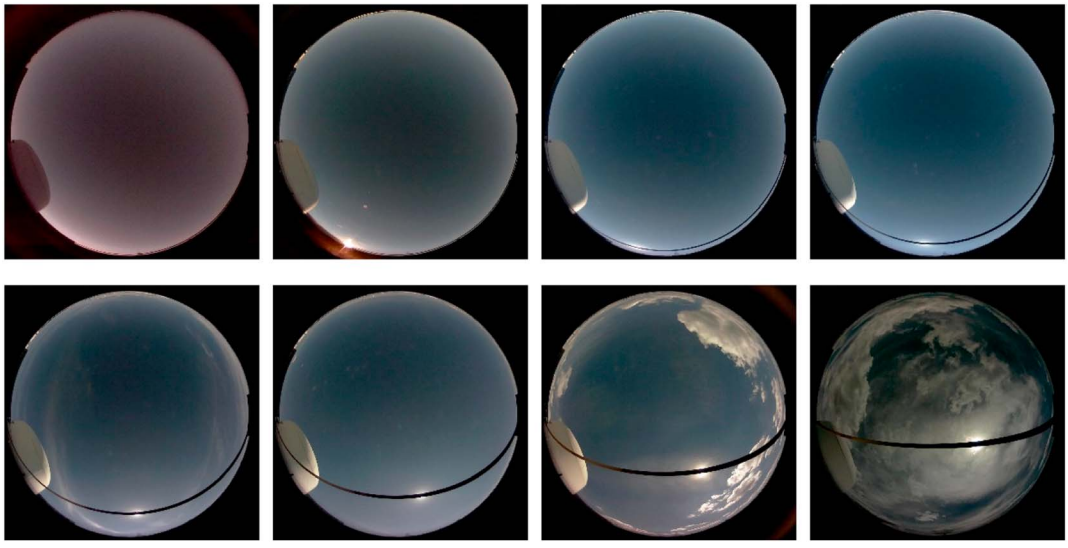

Figure 8. The total sky images on 22 June 2017. (top row) Images per hour from 9:00 to 12:00 and (bottom row) images per hour from 13:00 to 16:00.

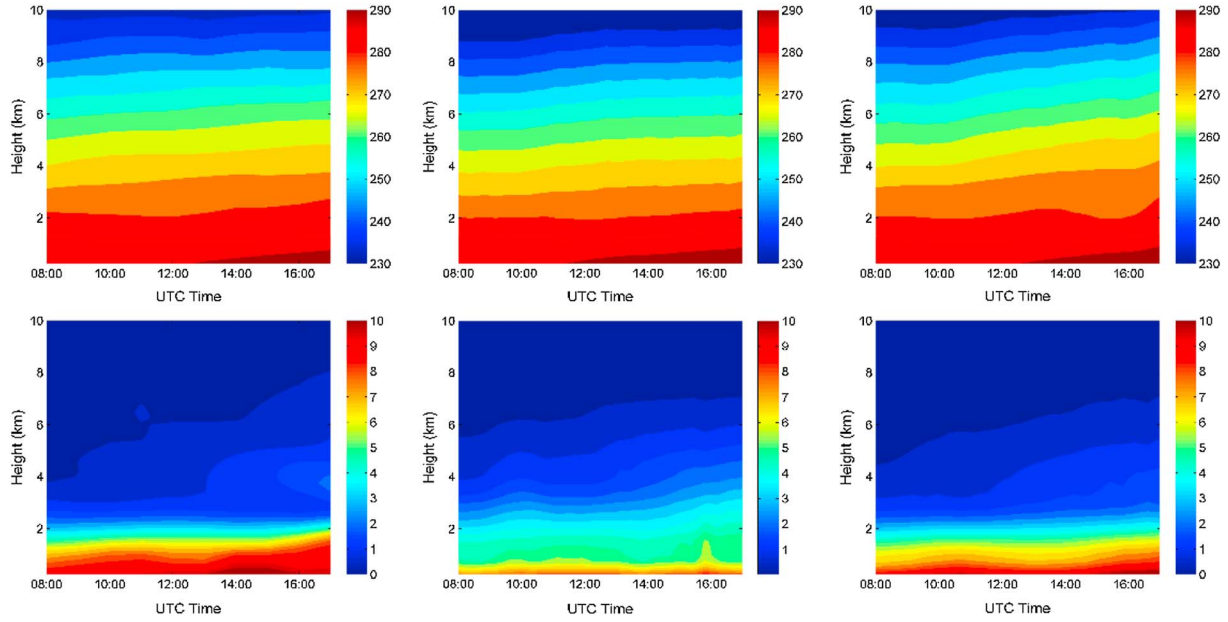

Figure 9. The continuous change of temperature and water vapor density on 22 June 2017. (left column) Rapid Refresh reanalysis, (middle column) neural network retrieval, and (right column) one-dimensional variational inversion. (top row) Temperature changes and (bottom row) records the evolution of water vapor density.

UTC 16:00 of that day are shown in Figure 8, indicating that the sky varied from clear sky to cloudy. The continuous inversion results of the NN (middle column) and the 1DVAR (right column) are illustrated in Figure 9. As a comparison, the original hourly refreshed RAP reanalysis is shown in the left column of Figure 9. Compared with the high-precision RAP temperature profiles, the NN inversion results are significantly lower, especially in the range of 2–8 km, which is consistent with the statistical error of the NN algorithm in Figure 7. The 1DVAR results have a good agreement with the temperature profile of the RAP except for just below the 2-km height at about 16:00. One possible reason for this is that we only consider the clear sky without taking into account the impacts of clouds on microwave radiation (the zenith is completely covered by cumulus clouds at 16:00; see last image of Figure 8). The accuracy of various methods is depicted more clearly by comparing their temperature retrieval results with RAOB for the case of UTC 12:00 (see left panel of Figure 10).

From the inversion of the water vapor density in Figure 9, the NN results are lower than the 1DVAR and the RAP below 2 km and slightly higher in the range of 2–6 km. Considering the RAP reanalysis profile itself has a

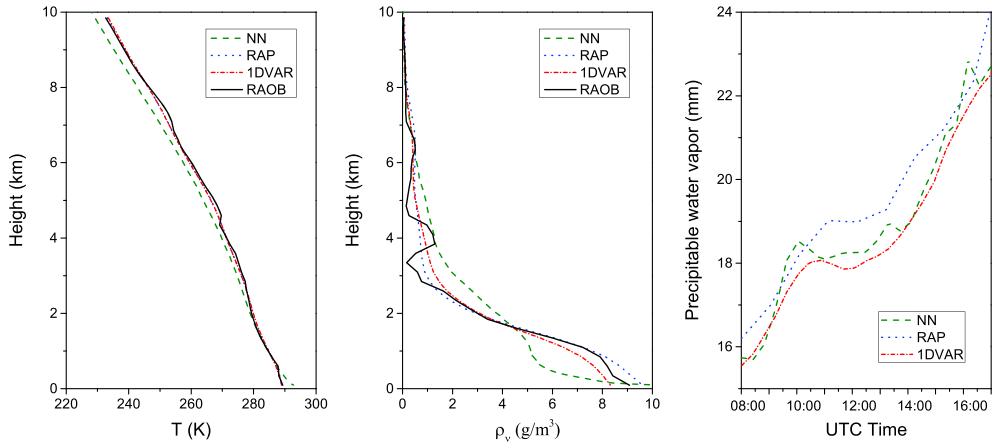

Figure 10. Comparison of neural network, Rapid Refresh, and one-dimensional variational retrieval with respect to radiosonde observations for the case of UTC 12:00 and their precipitable water vapors (PWVs) for the continuous retrieval on 22 June 2017. (left) Temperature inversion, (middle) inversion for water vapor density, and (right) PWVs.

certain deviation in the water vapor density, it is difficult to determine which retrieval algorithm is more accurate when merely comparing profiles with the RAP. On the one hand, we compared the difference between the inversion results of various methods with the RAOB (the middle panel of Figure 10). On the other hand, we calculated PWVs of the three methods for the whole continuous inversion period and their results are displayed in the right panel of Figure 10. We have assessed the PWVs of the RAP, NN, and 1DVAR in Table 1, which shows that the NN algorithm is reliable in the inversion of PWV. The PWVs of the NN and 1DVAR are in relatively good agreement, which indicates that the PWVs from the integrated 1DVAR profile should be credible. Contrarily, the PWVs of the RAP are, in most cases, significantly higher than those of the NN and 1DVAR. This indicates that the water vapor density profile of RAP is generally higher than the true value. Although the NN algorithm may be feasible for PWV inversion, the NN inversion accuracy of the water vapor density profile is poor, especially at low levels and high in the upper levels. In general, the accuracy of the 1DVAR profile inversion should be the most accurate among the three approaches.

5. Conclusions

There is an urgent need for accurate atmospheric vertical state information with a high temporal resolution for numerical weather forecasting model initialization and validation. NYS Mesonet, with its 17 enhanced instrument suites across NYS, has shown great promise in this regard. More specifically, NYS Mesonet MWRPs provide a good opportunity for real-time continuous inversion of temperature and humidity profiles in the lower atmosphere. However, the MWRP built-in NN algorithm has large retrieval errors both in temperature and humidity profiles. To meet the requirements of NYS Mesonet, we developed a new physics-based 1DVAR algorithm to retrieve the vertical distribution of temperature and water vapor density by combining ground-based MWRP measurements with RAP reanalysis profiles. Specifically, the 1DVAR algorithms based on an accurate PAM-VRT model as the forward radiation simulation and computed weighting functions for all MWRP microwave channels. Based on statistical analyses of gas absorption line models and MWRP calibration and observations, we concluded that the Liebe89 model is an accurate absorption line model for all cases tested. Furthermore, as the retrieval kernel is weighted toward the lower atmosphere, we only focused on profiles below 10 km. Consequently, we developed an integrated correction scheme to remove the radiation contribution from the upper atmosphere ($>$10 km). Based on the optimization theory (Rodgers, 1976), we constructed a retrieval algorithm that optimizes results between observational information (and associated measurement errors) and background information and error covariance. This physics-based 1DVAR algorithm has been further evaluated and validated for multiple month observations from the roof of the ASRC.

Based on the case analysis and statistical comparison of the three methods (1DVAR retrievals, the MWRP built-in NN retrievals, and RAP reanalysis) with RAOB, we concluded the following:

1. The maximum deviation between the RAP reanalysis temperature profile and RAOB is less than 0.3 K. Using MWRP measurements, more accurate temperature profiles can be achieved with the 1DVAR algorithm, particularly in the lower atmosphere ($<$4 km). The maximum deviation is less than 0.2 K; however, the temperature profile retrieved from the NN algorithm had a greater deviation in almost all levels with a maximum error greater than 3 K.
2. The water vapor density profiles of RAP reanalysis are generally higher than the true values. The inversion errors of the 1DVAR algorithm for water vapor density are significantly improved over the RAP reanalysis profile at almost all levels, and the maximum mean error and rms error are down from 0.5 and 1.0 g/m^3 to 0.15 and 0.7 g/m^3, respectively. Similar to the temperature profile retrievals, the NN retrieval had the greatest errors for both mean and rms, with the maximum deviation of the NN occurring at about a height of 1 km, a maximum mean error of 1.25 g/m^3, and a maximum rms error of 1.75 g/m^3, respectively. In general, the mean error of the NN indicates that the result of its inversion is lower than the RAOB below 2 km and higher than the RAOB above 2 km.
3. PWVs from RAP reanalysis are higher than RAOB measurements. The PWV retrieved from 1DVAR and NN algorithms are in relatively good agreement.

The results suggest that the 1DVAR retrievals, which combined both the MWRP observations and background field information, are superior to the NN retrievals as well as the RAP reanalysis. The overestimation of water vapor in RAP reanalysis compared with RAOB measurements, concluded from our statistical study, is also

important for the weather and climate community. In general, the 1DVAR algorithm can improve the accuracy of humidity profiles within 10 km, while improvements within temperature profiles occur mainly in the lower atmosphere (<4 km). This was determined by the properties of the Jacobian matrix and estimated background error covariance. Due to large errors in both humidity and temperature profiles, all atmospheric indices based on NN retrievals may contain substantial errors.

The background error covariance matrix B and the observation error covariance matrix R are very important for a successful and accurate inversion of the 1DVAR algorithm. In this study, we simply adopted the same B and R for all retrieval cases. For cases at different seasons, B and R should be dynamically adjusted to avoid unsuccessful convergence or excessive errors. In addition, the proposed 1DVAR algorithm obtained satisfactory inversion accuracy under clear skies; however, it was found that there will be large inversion errors when clouds develop in the zenith direction (see Figure 9 for temperature inversion). The critical issue is the cloud layer temperature. The inversion of atmospheric vertical parameters under cloudy sky conditions will require further analysis in the near future.

Acknowledgments

This work complies with the AGU data policy; the data used in this study can be obtained from http://doi.org/10.5281/zenodo.1220576. We gratefully acknowledge the support from the National Natural Science Foundation of China (41675030). We are also grateful for the funding provided by the U.S. National Science Foundation under grants AGS-1608735 and PIRE-1545917, by the NOAA Educational Partnership Program with Minority Serving Institutions (EPP/MSI) under cooperative agreement NA11SEC4810003, and by NASA's ROSES program element for DSCOVR Earth Science Algorithms. This research is made possible by the New York State (NYS) Mesonet. Original funding for the NYS Mesonet was provided by Federal Emergency Management Agency grant FEMA-4085-DR-NY, with the continued support of the NYS Division of Homeland Security & Emergency Services; the state of New York; the Research Foundation for the State University of New York (SUNY); the University at Albany, SUNY; the Atmospheric Sciences Research Center (ASRC) at SUNY Albany; and the Department of Atmospheric and Environmental Sciences (DAES) at SUNY Albany.

References

Araki, K., Murakami, M., Ishimoto, H., & Tajiri, T. (2015). Ground-based microwave radiometer variational analysis during no-rain and rain conditions. *Scientific Online Letters on the Atmosphere*, *11*, 108–112.

Benjamin, S. G., Weygandt, S. S., Brown, J. M., Hu, M., Alexander, C. R., Smirnova, T. G., et al. (2016). A north American hourly assimilation and model forecast cycle: The Rapid Refresh. *Monthly Weather Review*, *144*(4), 1669–1694. https://doi.org/10.1175/MWR-D-15-0242.1

Blackwell, W. J. (2005). A neural-network technique for the retrieval of atmospheric temperature and moisture profiles from high spectral resolution sounding data. *IEEE Transactions on Geoscience and Remote Sensing*, *43*(11), 2535–2546. https://doi.org/10.1109/TGRS.2005.855071

Blumstein, D., Chalon, G., Carlier, T., Buil, C., Hebert, P., Maciaszek, T., et al. (2004). IASI instrument: Technical overview and measured performances. Infrared Spaceborne Remote Sensing XII. In M. Strojnik (Ed.), *Proceedings on International Society for Optical Engineering* (Vol. 5543, pp. 196–207). Denver, CO: SPIE. https://doi.org/10.1117/12.560907

Boukabara, S. A., Garrett, K., Chen, W., Iturbide-Sanchez, F., Grassotti, C., Kongoli, C., et al. (2011). MiRS: An all-weather 1DVAR satellite data assimilation and retrieval system. *IEEE Transactions on Geoscience and Remote Sensing*, *49*(9), 3249–3272. https://doi.org/10.1109/TGRS.2011.2158438

Cadeddu, M. P., Turner, D. D., & Liljegren, J. C. (2009). A neural network for real-time retrievals of PWV and LWP from arctic millimeter-wave ground-based observations. *IEEE Transactions on Geoscience and Remote Sensing*, *47*(7), 1887–1900. https://doi.org/10.1109/TGRS.2009.2013205

Cimini, D., Campos, E., Ware, R., Albers, S., Giuliani, G., Oreamuno, J., et al. (2011). Thermodynamic atmospheric profiling during the 2010 Winter Olympics using ground-based microwave radiometry. *IEEE Transactions on Geoscience and Remote Sensing*, *49*(12), 4959–4969. https://doi.org/10.1109/TGRS.2011.2154337

Cimini, D., Westwater, E. R., & Gasiewski, A. J. (2010). Temperature and humidity profiling in the Arctic using millimeter-wave radiometry and 1DVAR. *IEEE Transactions on Geoscience and Remote Sensing*, *48*(3), 1381–1388. https://doi.org/10.1109/TGRS.2009.2030500

Culverwell, I. D., Lewis, H. W., Offiler, D., Marquardt, C., & Burrows, C. P. (2015). The radio occultation processing package, ROPP. *Atmospheric Measurement Techniques*, *8*(4), 1887–1899. https://doi.org/10.5194/amt-8-1887-2015

Desportes, C., Obligis, E., & Eymard, L. (2010). One-dimensional variational retrieval of the wet tropospheric correction for altimetry in coastal regions. *IEEE Transactions on Geoscience and Remote Sensing*, *48*(3), 1001–1008. https://doi.org/10.1109/TGRS.2009.2031494

Duncan, D. I., & Kummerow, C. D. (2016). A 1DVAR retrieval applied to GMI: Algorithm description, validation, and sensitivities. *Journal of Geophysical Research: Atmospheres*, *121*(12), 7415–7429. https://doi.org/10.1002/2016JD024808

Hewison, T. (2007). 1D-VAR retrievals of temperature and humidity profiles from a ground-based microwave radiometer. *IEEE Transactions on Geoscience and Remote Sensing*, *45*(7), 2163–2168. https://doi.org/10.1109/TGRS.2007.898091

Jang, H. S., Sohn, B. J., Chun, H. W., Li, J., & Weisz, E. (2017). Improved AIRS temperature and moisture soundings with local a priori information for the 1DVAR method. *Journal of Atmospheric and Oceanic Technology*, *34*(5), 1083–1095. https://doi.org/10.1175/JTECH-D-16-0186.1

Keihm, S. J., & Marsh, K. A. (1996). Advanced algorithm and system development for Cassini radio science tropospheric calibration. Telecommunication and data acquisition Prog. Rept. 42–127, 1–20, Pasadena, CA: Jet Propulsion The Laboratory.

Liebe, H. J. (1989). MPM—An atmospheric millimeter-wave propagation model. *International Journal of Infrared and Millimeter Waves*, *10*(6), 631–650. https://doi.org/10.1007/BF01009565

Liebe, H. J., Hufford, G. A., & Cotton, M. G. (1993). Propagation modeling of moist air and suspended water/ice particles at frequencies below 1000 GHz. *AGARD Conference Proceedings*, *542*, 3.1–3.10.

Liljegren, J. C. (2000). Automatic self-calibration of ARM microwave radiometers. In P. Pampaloni, & S. Paloscia (Eds.), *Microwave radiometry and remote sensing of the Earth's surface and atmosphere* (pp. 433–443). Lorton, VA: VSP Book.

Lin, B., Minnis, P., Fan, A., Curry, J. A., & Gerber, H. (2001). Comparison of cloud liquid water paths derived from in situ and microwave data taken during the SHEBA/FIREACE. *Geophysical Research Letters*, *28*(6), 975–978. https://doi.org/10.1029/2000GL012386

Liu, Q., & Weng, F. (2005). One-dimensional variational retrieval algorithm of temperature, water vapor, and cloud water profiles from advanced microwave sounding unit (AMSU). *IEEE Transactions on Geoscience and Remote Sensing*, *43*, 1087–1095.

Martinet, P., Cimini, D., De Angelis, F., Canut, G., Unger, V., Guillot, R., et al. (2017). Combining ground-based microwave radiometer and the AROME convective scale model through 1DVAR retrievals in complex terrain: An Alpine valley case study. *Atmospheric Measurement Techniques*, *10*(9), 3385–3402. https://doi.org/10.5194/amt-10-3385-2017

Mattioli, V., Westwater, E. R., Cimini, D., Gasiewski, A. J., Klein, M., & Leuski, V. (2008). Microwave and millimeter-wave radiometric and radiosonde observations in an arctic environment. *Journal of Atmospheric and Oceanic Technology*, *25*(10), 1768–1777. https://doi.org/10.1175/2008JTECHA1078.1

Rodgers, C. D. (1976). Retrieval of atmospheric temperature and composition from remote measurements of thermal radiation. *Reviews of Geophysics and Space Physics*, *14*(4), 609–624. https://doi.org/10.1029/RG014i004p00609

Rodgers, C. D. (2000). *Inverse methods for atmospheres: Theory and practice*. Singapore: World Scientific Publishing. https://doi.org/10.1142/3171

Rosenkranz, P. W. (1998). Water vapor continuum absorption: A comparison of measurements and models. *Radio Science*, *33*(4), 919–928. https://doi.org/10.1029/98RS01182

Sanò, P., Panegrossi, G., Casella, D., Di Paola, F., Milani, L., Mugnai, A., et al. (2015). The passive microwave neural network precipitation retrieval (PNPR) algorithm for AMSU/MHS observations: Description and application to European case studies. *Atmospheric Measurement Techniques*, *8*(2), 837–857. https://doi.org/10.5194/amt-8-837-2015

Solheim, F., Godwin, J. R., Westwater, E. R., Han, Y., Keihm, S. J., Marsh, K., & Ware, R. (1998). Radiometric profiling of temperature, water vapor, and cloud liquid water using various inversion methods. *Radio Science*, *33*(2), 393–404. https://doi.org/10.1029/97RS03656

Westwater, E. R. (1993). Ground-based microwave remote sensing of meteorological variables. In M. Janssen (Ed.), *Atmospheric remote sensing by microwave radiometry* (pp. 145–213). New York, NY: John Wiley.

Yang, J., & Min, Q. (2015). A passive and active microwave-vector radiative transfer (PAM-VRT) model. *Journal of Quantitative Spectroscopy & Radiative Transfer*, *165*, 123–133. https://doi.org/10.1016/j.jqsrt.2015.06.028

Yang, J., Min, Q., Lu, W., Ma, Y., Yao, W., & Lu, T. (2017). An RGB channel operation for removal of the difference of atmospheric scattering and its application on total-sky cloud detection. *Atmospheric Measurement Techniques*, *10*(3), 1191–1201. https://doi.org/10.5194/amt-10-1191-2017

Yang, J., Min, Q., Lu, W., Ma, Y., Yao, W., Lu, T., et al. (2016). A total sky cloud detection method using real clear sky background. *Atmospheric Measurement Techniques*, *9*(2), 587–597. https://doi.org/10.5194/amt-9-587-2016